ELSEVIER

Journal of Organometallic Chemistry 648 (2002) 14–26

Journal of Organometallic Chemistry

www.elsevier.com/locate/jorganchem

A theoretical analysis of [M(tmtaa)] and [M(acacen)] fragments employed in the organometallic chemistry of early transition metals

Paola Belanzoni, Marzio Rosi *, Antonio Sgamellotti

Dipartimento di Chimica, Centro per il Calcolo Intensivo in Scienze Molecolari, Università di Perugia, via Elce di Sotto 8, I-06123 Perugia, Italy

Received 28 May 2001; accepted 5 November 2001

Abstract

The [M(tmtaa)] and [M(acacen)] fragments employed in the organometallic chemistry of titanium and vanadium have been investigated by a density functional approach. The frontier orbitals and the geometrical structure of the two macrocyclic ligands have been compared and the effect of the nature of the metal on the ligand environments has been studied. Some interesting complexes in which the metal contains a reactive organometallic functionality, such as metal–halogen (F and Cl) or metal–alkyl (CH_3) units, have been investigated. Moreover, the $[Mo(acacen)]_2$ dimer has been considered because of its interest as a metal–metal bonded complex with non-bridging ligands restraining the metal–metal distance.

Keywords: Density functional calculations; *N*,*N*′-ethylenebis(acetylacetoneiminato)dianion Schiff base ($[acacen]^{2-}$); Dibenzotetramethyltetraaza[14]annulene dianion ($[tmtaa]^{2-}$); Early transition metal complexes

1. Introduction

The study of polydentate macrocyclic ligands represent a vast area of chemical and biochemical research under broad development during the last number of years. The attraction of these macrocyclic ligands is due to the fact that they can not only offer a wide variety of donor atom types, ligand charges, coordination numbers and resultant complex geometries, but that the macrocyclic complexes can also exhibit enhanced kinetic and thermodynamic stability in comparison with those of monodentate ligands [1,2].

The present paper will deal with two tetradentate macrocyclic ligands as the *N*,*N*′-ethylenebis(acetylacetoneiminato)dianion Schiff base ($[acacen]^{2-}$) and the dibenzotetramethyltetraaza[14]annulene dianion ($[tmtaa]^{2-}$) and with their early transition metal complexes, namely titanium [3,4] and vanadium [5,6] derivatives. Transition metal complexes of these two ligands have received much recent attention as potential alternatives to the ubiquitous bis(η-cyclopentadienyl) ligand set and, in particular, the organometallic and coordination chemistry of early transition metal complexes has been extensively developed by the Floriani and Jordan groups [7–15]. The late transition metal complexes are very similar to some biological systems and act as precursors of polymeric electroactive films. The macrocyclic complexes of the middle to late transition metals have continued to be studied, in the area of bioinorganic chemistry, as models for the active sites of certain naturally-occurring enzymes. Electrochemical studies of middle to late transition metal macrocyclic complexes can lead to the synthesis of new materials since modification of the ring substituents can affect the redox properties of the complexes and influence their tendency to form dimeric or polymeric systems.

The chemistry of unbridged $[M(tmtaa)]_2$ or $[M(acacen)]_2$ type dimers is small in comparison to the large field of monomeric species. These metal–metal bonded complexes with non-bridging macrocycles warrant more study in view of their stability despite the potential steric repulsions of the macrocyclic ligands. Furthermore, these porphyrin-like systems have potential as

* Corresponding author. Fax: +39-075-5855606.
E-mail address: marzio@thch.unipg.it (M. Rosi).

0022-328X/02/$ - see front matter
PII: S0022-328X(01)01445-0

catalysts in redox processes. Since a $[Mo(acacen)]_2$ complex has been synthesized [16] we decided to study this dimeric species from a theoretical point of view and to compare it with the theoretically characterized complex $[Mo(tmtaa)]_2$ [17].

The title macrocyclic ligands share many common structural characteristics with porphyrins. The tmtaa ligand, similarly to porphyrins, has four coplanar nitrogen atoms and a completely conjugated system of double bonds; the acacen ligand has two nitrogen atoms and two oxygen atoms on the same plane and a system of double bonds. Upon transition metal complexation the two macrocyclic ligands show some differences with porphyrins, more noticeable for tmtaa. While porphyrin retains a planar structure with the metal lying on the same plane as the four nitrogen atoms, a saddle shape conformation is produced for tmtaa and this causes displacement of the coordinated metal out from the N_4 plane; for acacen, a planar conformation is retained and the coordinated metal is only slightly displaced from the N_2O_2 plane. The degree of non-planarity of the macrocyclic tmtaa in its metal complexes depends on different factors, such as the radius and d-electron count of the metal ion itself and, to a lesser extent, the number and type of any axial ligands. An important consequence of the saddle shape conformation of the metal coordinated tmtaa is that of favoring five-coordination over six-coordination.

While the late transition metal tmtaa and acacen complexes have been extensively studied (see for example [18]), the early transition metal analogues need still to be theoretically characterized [19].

2. Computational details

The calculations reported in this paper are based on the ADF (Amsterdam Density Functional) program [20–24]. The main characteristics of this computational package are the use of a density fitting procedure to obtain accurate Coulomb and exchange potentials in each self-consistent field (SCF) cycle, the accurate and efficient numerical integration of the effective one-electron Hamiltonian matrix elements, and the possibility to freeze core orbitals. The molecular orbitals were expanded in uncontracted Slater-type atomic orbitals. The following orbitals were kept frozen in the core: C(1s); N(1s); O(1s); F(1s); Ti(1s-2p); V(1s-2p); Cl(1s-2p); Mo(1s-4p). The valence basis set we used is described as a double-ζ plus polarization quality basis set for all atoms with the exception of the Ti, V and Mo for which we chose a triple-ζ plus polarization basis set. As polarization functions one 2p STO was used for H, one 3d for C, N, O, F and Cl atoms, one 4p for Ti and V, and one 5p for Mo. Singlet ground states were calculated by spin restricted approach, while higher spin ground states by spin unrestricted treatment. The spin multiplicity of the ground state has been accurately checked for all the investigated systems. The LDA exchange potential and energy were used, in the Vosko et al. [25] parametrization for homogeneous electron gas correlation, including the Perdew's non-local correction [26] for correlation and the Becke's non-local correction [27] to the local exchange expression.

In order to simplify the theoretical analysis tmtaa and acacen are replaced by model systems shown in Scheme 1.

The methyl groups are replaced by hydrogen and, due to the lack of conjugation between the 1,3-diiminato and *o*-phenylene fragments, *o*-C_6H_4 can be successfully substituted by *cis*-C_2H_2 [8,18,28]. Moreover, in acacen, the sp^3 carbons bridging the nitrogen atoms are forced to lie in the N_2O_2 plane to preserve the highest possible symmetry. Due to this constraint, the CCN angle shifts from 109 to 114°. The structures of tmtaa and acacen are usually non-planar. For tmtaa this is generally attributed to the steric interactions of the methyl groups in the 1,3-diiminato linkages with the benzenoid rings [29]. In their metal complexes, tmtaa has a pronounced saddle shape, with the two 1,3-diiminato chelates bending down and the two benzenoid rings warping up (i.e. towards the metal coordination site), while acacen shows slight twisting of the N_2O_2 core, and the metal atom lies out of the N_4 and, to a small extent, out of the N_2O_2 planes. In our calculations the molecular structures of tmtaa and acacen dianionic ligands were taken from the experimental X-ray crystallographic data of the corresponding vanadium chloride derivatives [9,30] and were partially optimized in C_{2v} symmetry for $[tmtaa]^{2-}$ and in C_s

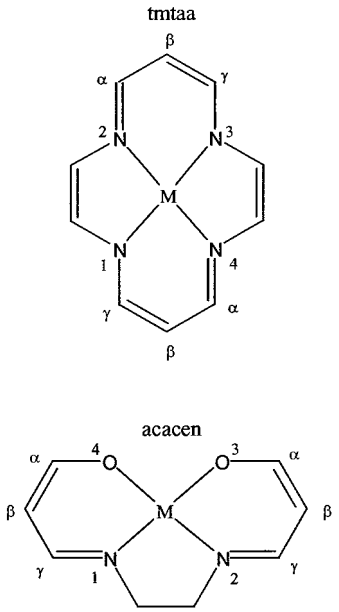

Scheme 1. Geometrical structures of the considered model ligands, $[tmtaa]^{2-}$ and $[acacen]^{2-}$.

Table 1
Frontier orbitals of the $[tmtaa]^{2-}$ and $[acacen]^{2-}$ ligands

Orbital	E (eV)	% N	% *cis*-C_2H_2	% $C_{\alpha,\gamma}$	% C_β
$[tmtaa]^{2-}$					
$10b_2$	6.447	$34(p_z)$		$28(p_z)$	
$8a_2$ LUMO	5.560	$11(p_x)$	$24(p_z)$	$24(p_z)+13(p_z)$	
$11a_1$ HOMO	4.055	$36(p_z)$	$18(p_z)$		$18(p_z)$
$9b_2$	3.274	$28(p_y)+11(2s)$			
$9b_1$	3.215	$26(p_x)+17(p_z)+10(p_y)$			$18(p_z)$
Orbital	E (eV)	% N	% O	% $C_{\alpha,\gamma}$	% C_β
$[acacen]^{2-}$					
$17a''$	6.804	$23(p_y)$	$18(p_y)$	$49(p_y)$	
$18a'$ LUMO	6.430	$16(p_y)$	$15(p_y)$	$46(p_y)$	
$16a''$ HOMO	4.109	$18(p_x)$	$34(p_x)$		
$17a'$	3.729		$44(p_x)$		
$15a''$	3.176	$30(p_y)$	$17(p_y)$		$38(p_y)$
$16a'$	2.904	$31(p_y)$	$18(p_y)$		$39(p_y)$

Only the main contributions are reported.

symmetry for $[acacen]^{2-}$. In particular, the dihedral angles have been frozen. Analogously, geometries of the corresponding metal complexes and metal complexes including additional X ligand have been partially optimized in C_{2v} or C_s symmetries.

For $[Mo(acacen)]_2$ compound calculations we used a model system, where the macrocyclic acacen ligand was simplified to that shown in Scheme 1 and the relevant bond distances, bond angles, and dihedral angles were taken from the experimental crystal structure of the real molecule [16], showing an Mo–Mo distance of 2.168 Å, and were averaged to conform to C_{2h} idealized symmetry.

3. Results and discussion

3.1. The $[tmtaa]^{2-}$ and $[acacen]^{2-}$ ligands

Density functional calculations have been performed to study the difference in the chemical environments provided by two macrocyclic ligands as the *N*,*N*′-ethylenebis(acetylacetoneiminato)dianion Schiff base ($[acacen]^{2-}$) and the dibenzotetramethyltetraaza-[14]annulene dianion ($[tmtaa]^{2-}$). In their mononuclear metal complexes, tmtaa and acacen behave as dianionic tetradentate ligands. Recently those two classes of tetradentate ligands have received much attention as potential alternatives to the ubiquitous bis (η-cyclopentadienyl) ligand set and have been used for studying M–C functionalities in the area of early transition metals [31–34].

At first we endeavor to understand the major differences existing between a N_4 and a N_2O_2 donor core in a square or near-square planar arrangement, respectively. As for the ligand geometries, it has been shown from previous calculations [18] that deformation from planarity on going from *taa* to *tmtaa* has negligible electronic effects on the nature and energy of the macrocycle orbitals involved in the interactions with the metal and for this reason for $[tmtaa]^{2-}$ only the distances between the nitrogen atoms, for $[acacen]^{2-}$ only the distances between nitrogen and oxygen atoms, have been optimized (see Section 2). The optimized distances (for the atom labels see Scheme 1) are for tmtaa $N_1–N_4 = N_2–N_3 = 2.780$, $N_1–N_2 = N_3–N_4 = 2.589$ Å and for acacen $N_1–N_2 = 2.710$, $O_3–O_4 = 3.117$ and $N_1–O_4 = N_2–O_3 = 2.401$ Å. The frontier orbitals of the two model dianionic ligands are shown in Table 1, where the percentage composition in terms of atomic orbitals is specified. Highest occupied and lowest unoccupied orbitals perpendicular to the N_4 (N_2O_2) plane are depicted in Fig. 1. The circles in the figure indicate the phase relationship of the top lobe of each π-orbital.

We can recognize two highest occupied and two lowest unoccupied orbitals which are characteristic of $[tmtaa]^{2-}$. Although these four orbitals are delocalized over the entire π system, they may be considered as primarily in-phase and out-of-phase combinations of π (or π*) orbitals of two 1,3-diiminato chelates. In particular, the two highest occupied orbitals of tmtaa, $11a_1$ and $9b_1$, contain contributions from the *meso*-carbon atoms of the 1,3-diiminato chelates, while the two lowest unoccupied orbitals, $8a_2$ and $10b_2$, contain contributions from the iminato (–C=N) carbon atoms of the same group. It should be noticed that the $9b_1$ orbital contains also contributions from the nitrogen p in-plane atomic orbitals. The ethylene-like carbons contribute to the $11a_1$ highest occupied orbital and $8a_2$ lowest unoccupied orbital compositions, while the

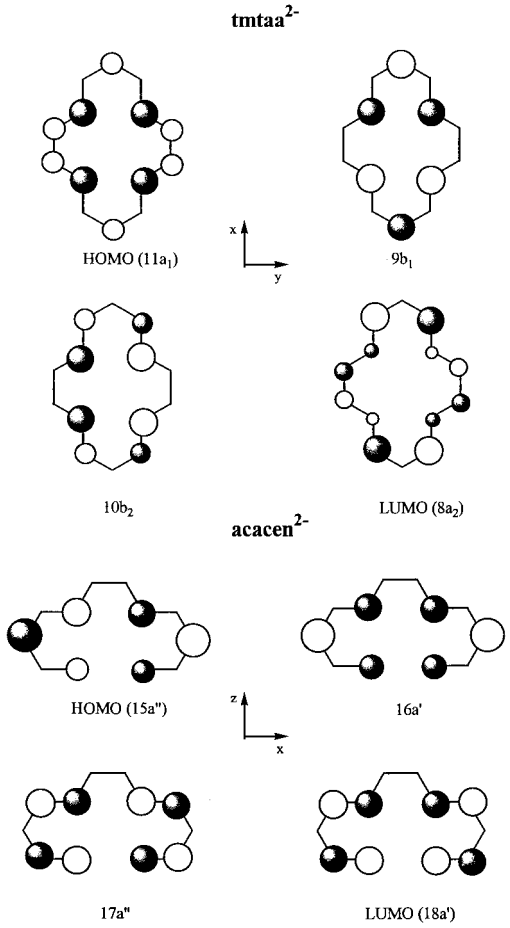

Fig. 1. Highest occupied and lowest unoccupied orbitals perpendicular to the N_4 (N_2O_2) plane of the simplified $[tmtaa]^{2-}$ and $[acacen]^{2-}$ ligands.

meso-carbon atoms of the 1,3-diiminato chelates do not enter in the composition of the virtual orbitals. The second highest occupied orbital, $9b_2$, omitted from the figure, is mainly localized over the nitrogen atoms in plane, without mixing significantly with any carbon atom.

The two highest occupied and the two lowest unoccupied orbitals characteristic of the $[acacen]^{2-}$ may be analogously considered as in-phase and out-of-phase combinations of π (or π*) orbitals of two five-membered chelates. Apart from the contributions from N_2O_2 core, the two highest occupied orbitals, 15a″ and 16a′, involve the *meso*-carbon atoms, while the two lowest unoccupied orbitals, 18a′ and 17a″, involve the carbon atoms connected to nitrogen and oxygen atoms (C_α and C_γ). The 17a′ orbital, not illustrated in Fig. 1, is mainly localized over the oxygen atoms in the plane of the ligand (*xz*) and can be described primarily as a p_x combination of oxygen orbitals. The highest occupied orbital 16a″ is principally localized over the nitrogen and oxygen atoms on the N_2O_2 plane.

Some further information can be provided by the Mulliken charge distribution analysis, which allows the localization of the electrophilic and the nucleophilic centers on the two ligands. For $[tmtaa]^{2-}$ the negative charge is distributed mainly over the four nitrogen atoms (-0.51) and at the *meso*-carbon atoms (-0.18), thus representing the electrophilic sites, while the iminato carbon atoms of the 1,3-diiminato chelates, carrying a partial positive charge ($+0.24$), act as nucleophilic centers. Only a small positive charge is seen at the carbon atoms of the ethylene-like groups ($+0.11$). For $[acacen]^{2-}$ the negative charge is delocalized over the N_2O_2 core, with a larger value on oxygen atoms (-0.67 vs. -0.55 at nitrogen) and significant deposits at the *meso*-carbon atoms of the five-membered chelation group (-0.25). The nucleophilic character of the carbon atoms connected to oxygen and nitrogen is increased ($+0.57$ at C–O and $+0.35$ at C–N) with respect to the corresponding iminato atoms in $[tmtaa]^{2-}$, and a small amount of positive charge is calculated on carbon atoms of the nitrogen bridging C_2H_4 group ($+0.15$). The ability of the iminato carbons to 'carry' some of the positive charge contributes also to the reduced electrophilicity of the $[Zr(Me_4taa)]^{2+}$ fragment versus the apparently related $[Zr(\eta\text{-}C_5H_5)_2]^{2+}$ [8].

The majority of the reaction chemistry of tmtaa complexes concerns changes at the metal center with the macrocycle acting only as a supporting ligand, while the most common site for reactions occurring at the ligand itself is at the *meso*-carbon atoms. The same behavior can be expected from acacen complexes. High oxidation state, early transition metal alkyl complexes (such as Zr) can undergo intramolecular migratory nucleophilic attack at an iminato carbon atom [8]. Lower oxidation state metal [e.g. Ti(III) and V(III)] alkyl complexes are however stable to this type of migration, possibly as a consequence of the reduced positive charge at the iminato carbon atoms.

3.2. The $[M(tmtaa)]^+$ and $[M(acacen)]^+$, M = Ti, V complexes

We introduce now early transition metal atoms (Ti and V) in those two macrocyclic environments, in order to investigate the effect of the nature of the metal on the ligands. Partial geometry optimization calculations have been done, in C_{2v} symmetry for $[M(tmtaa)]^+$ and in C_s symmetry for $[M(acacen)]^+$ complexes, to optimize the distances between the metal and the N_4 or N_2O_2 plane and between the atoms constituting the N_4 or N_2O_2 plane. The results are shown in Table 2. The frontier orbitals of the four related organometallic fragments are illustrated in Fig. 2.

The MO treatment applied to these complexes allows the analysis of the energy level diagram and hence the

Table 2
Optimized geometrical distances (in Å) for $[M(tmtaa)]^+$ and $[M(acacen)]^+$ M = Ti, V complexes

$[Ti(tmtaa)]^+$ Distance		$[V(tmtaa)]^+$ Distance	
N_1–N_4 (≡N_2–N_3)	2.727	N_1–N_4 (≡N_2–N_3)	2.705
N_1–N_2 (≡N_3–N_4)	2.576	N_1–N_2 (≡N_3–N_4)	2.565
Ti–N	2.020	V–N	1.977
$[Ti(acacen)]^+$ Distance		$[V(acacen)]^+$ Distance	
N_1–N_2	2.822	N_1–N_2	2.673
O_3–O_4	3.182	O_3–O_4	2.989
N_1–O_4 (≡N_2–O_3)	2.429	N_1–O_4 (≡N_2–O_3)	2.827
Ti–N	1.866	V–N	1.949
Ti–O	2.006	V–O	2.060

interpretation of the 'ligand field' effect acting on the central transition metal. Obviously, since the d-orbitals mix strongly with the tmtaa and acacen frontier orbitals, no pure d-orbital can be assigned. However, 'five metal d-based orbitals' can be recognized, where the d character is large. The metal d-orbitals of the formally V(III) species with a d^2 configuration and bonded to tmtaa are depicted in the second column of Fig. 2. The d_{xy}-orbital ($9a_2$), which more strongly interacts with the N lone pairs of the tmtaa ligand, pointing towards the atoms of the N_4 core, is pushed quite high in energy, leaving as the lowest metal orbital the $14a_1$ (d_{z^2}), stabilized by the lacking of axial ligands and fully occupied. The $15a_1$ and $11b_1$ ($d_{x^2-y^2}$ and d_{xz}, respectively) orbitals are close in energy and lie ca. 0.2 and 0.3 eV, respectively, above the d_{z^2}. On the other hand, the energy separation between the $12b_2$ (d_{yz}) and $14a_1$ (d_{z^2}) orbitals is ca. 1.8 eV, due to the repulsive interaction of the d_{yz} orbital with the ligand orbital of the same symmetry ($11b_2$). Two tmtaa LUMO's character orbitals ($8a_2$ and $11b_2$) are localized in energy just above the $14a_1$ orbital and, as noted before, $11b_2$ is slightly mixed with d_{yz} metal orbital.

The frontier orbitals of $[Ti(tmtaa)]^+$ (d^1 configuration) are depicted in the first column of Fig. 2, and are quite similar to those calculated in the corresponding vanadium fragment, as we could expect, since we are considering the same ligand. Therefore, when comparing the electronic structure of titanium and vanadium

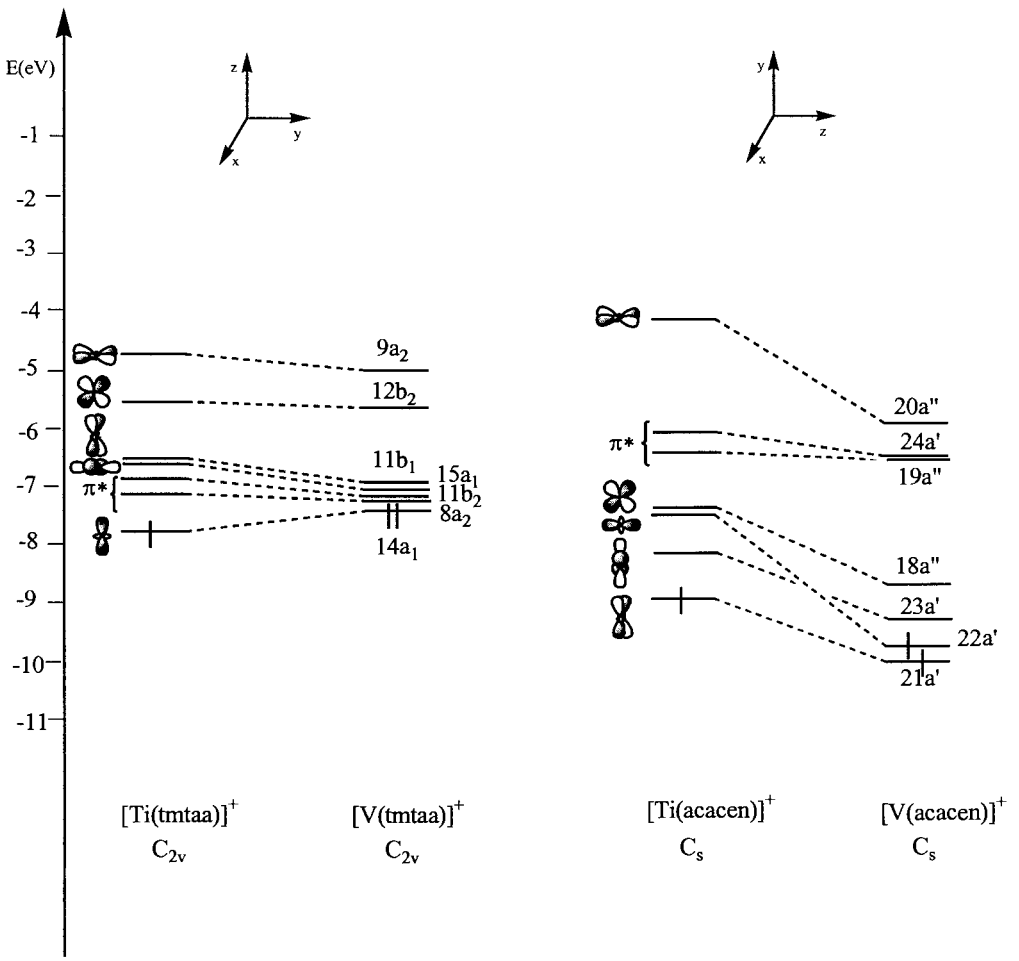

Fig. 2. Frontier orbitals of the $[Ti(tmtaa)]^+$, $[V(tmtaa)]^+$, $[Ti(acacen)]^+$ and $[V(acacen)]^+$ fragments.

tetraazamacrocycles the only noticeable difference is a downward energy shift of the metal orbitals when going from titanium to vanadium.

The frontier orbitals for the d^2 $[V(acacen)]^+$ organometallic fragment are depicted in the last column of Fig. 2. They are quite different from those calculated in the corresponding tmtaa fragment, the main difference consisting in a larger separation between the orbitals which span a broader range of energy, thus indicating a stronger interaction between metal and ligand orbitals. The d_{xz}-orbital (20a″), interacting with the acacen N and O centers lone pairs, is strongly destabilized, while the d_{z^2} (22a′) and d_{xy} (21a′) orbitals, not interacting with ligand orbitals, are stabilized and result each in single occupation. The LUMO's acacen character orbitals (19a″ and 24a′) are pushed higher in energy, due to the stronger interaction with the metal which is at a smaller distance to the ligand pseudo-plane and, consequently, the 23a′ and 18a″, which are $d_{x^2-y^2}$ and d_{yz} metal orbitals, are stabilized but still lie above the d_{z^2} (22a′) and d_{xy} (21a′) orbitals.

A very similar orbital pattern is shown by the [Ti(acacen)]$^+$ analogue, with the same energy order of the d-orbitals except for the empty d_{z^2}-orbital which is destabilized and pushed in energy between the $d_{x^2-y^2}$ and the d_{yz} by the overlap with the π system of the ligand, caused again by the short distance of the metal to the ligand pseudo-plane. Shorter distances between the metal and the ligand N and O centers are reported for the Ti system, thus the d_{z^2}-orbital showing a larger destabilization for the latter system. Note also that the metal d character orbitals in the $[V(acacen)]^+$ are shifted down in energy respect to $[Ti(acacen)]^+$ fragment.

Substantially, no important difference in the frontier orbital patterns between these classes of compounds exists: the $[M(tmtaa)]^+$ fragment has four low-lying metal d-orbitals (d_{z^2}, $d_{x^2-y^2}$, d_{xz}, d_{yz}) available for additional ligands (see coordinate system in Fig. 1) and two low-lying empty orbitals localized on the tmtaa imine carbons; analogously, the $[M(acacen)]^+$ fragment has four metal-based frontier orbitals (d_{xy}, $d_{x^2-y^2}$, d_{z^2}, d_{yz}) and two higher-lying empty orbitals localized on the acacen α and γ carbons available for additional ligands. Not only the number of low-lying metal orbitals is the same in the two fragments, but also the spatial extension of these orbitals does not permit the clear identification of the preference for a *cis* or *trans* coordination of two additional ligands. Therefore, the similarity in frontier orbital patterns existing between those two classes of tetradentate ligands explains why they show similar conformation in their complexes. However, two major differences exist between tmtaa and acacen. One is the significantly shorter metal to ligand pseudo-plane distance in acacen molecules than in tmtaa molecules. The other difference lies in the number of π electrons. A tmtaa dianion ligand carries 16 π electrons and can be described as a conjugated, anti-aromatic ($4n$) system; the acacen dianion ligand has 12 π electrons, it is non-cyclic and has a saturated ethylene group. The negative charge of tmtaa dianion is considered to be delocalized over the α-γ-pentadiiminato chelates, and in acacen is considered to be delocalized over the α-γ-pentadiiminato chelate and partially localized on oxygen atoms.

In the molecular shape and coordination conformation preference $[M(tmtaa)X_2]$ bears more resemblance with the $[Cp_2MX_2]$ compounds, while $[M(acacen)X_2]$ can be considered more similar to porphyrins. However, among the important differences existing between $[M(tmtaa)X_2]$ and $[Cp_2MX_2]$ classes of compounds [14], the experimental evidence should be mentioned here which emphasizes the major difference of chemical reactivity between the V-R functionality, when bonded to the [V(tmtaa)] or the $[Cp_2V]$ fragment [9], namely the insertion of carbon monoxide reaction. While for $[Cp_2V]$ the reaction leads to the corresponding acylcarbonyl derivatives, for [V(tmtaa)] it gives rise to a oxovanadium complex through an intermediate acyl where V interacts in a η^2-bonding mode with C=O. The formation of this intermediate can be easily explained by the frontier orbital pattern shown in the second

Table 3
Optimized geometrical distances (in Å) for [M(tmtaa)X] and [M(acacen)X] M = Ti, V and X = F, Cl, CH_3 complexes

Complex	Distance	L = tmtaa	L = acacen
TiLF	Ti–N	2.033	1.931
	Ti–O		2.054
	Ti-plane	0.771	0.530
	Ti–F	1.801	1.809
TiLCl	Ti–N	2.025 (2.060)	1.907
	Ti–O		2.031
	Ti-plane	0.763 (0.785)	0.365
	Ti–Cl	2.263 (2.293)	2.267
$TiLCH_3$	Ti–N	2.024	1.893 (2.121)
	Ti–O		2.020 (1.927)
	Ti-plane	0.739	0.498 (0.499)
	Ti–CH_3	2.105	2.115 (2.216)
VLF	V–N	2.002	1.883
	V–O		2.009
	V-plane	0.682	0.222
	V–F	1.771	1.789
VLCl	V–N	1.981 (2.009)	1.882 (2.062)
	V–O		2.011 (1.949)
	V-plane	0.597 (0.644)	0.172 (0.143)
	V–Cl	2.227 (2.221)	2.230 (2.352)
$VLCH_3$	V–N	1.989 (2.006)	1.871 (2.025)
	V–O		2.003 (1.925)
	V-plane	0.581 (0.570)	0.437 (0.421)
	V–CH_3	2.071 (2.073)	2.057 (2.064)

Experimental values are given in parentheses [7,9,30,31].

column of Fig. 2; the empty low-lying $11b_2$, partially d_{yz} in character, can act as a σ acceptor orbital toward the CO, oriented along the *y*-axis, while the HOMO with some $d_{x^2-y^2}$ character orbital can be involved in the back-donation π-interaction (V along the *z*-axis, tmtaa lying on the *xy* plane).

An analysis of the Mulliken charges of $[M(tmtaa)]^+$ fragments shows an increase of the negative charges at the nitrogen atoms (from −0.51 to −0.75 for Ti and −0.72 for V), while the negative charge at the *meso*-carbon atoms remains unchanged, and an enhanced positive charge at the carbons of the C_2H_2 groups (from +0.11 to +0.14 for Ti and +0.16 for V), while the positive charge at the iminato carbon atoms is only slightly increased (from +0.24 to +0.28 for Ti and +0.31 for V). The most electrophilic center in these fragments is the metal, which bears the highest positive charge, +1.64 for Ti and +1.33 for V. Therefore, the metal should undergo direct attack by the base (nucleophile). For $[M(acacen)]^+$ fragments, the negative charge is enhanced at the nitrogen (from −0.55 to −0.85 for Ti and −0.82 for V), at the oxygen (from −0.67 to −0.81 for Ti and −0.77 for V) and reduced at the *meso*-carbon atoms (from −0.18 to −0.13 for Ti and −0.11 for V), while significant reduction of the positive charge is seen at the C_2H_4 carbons (from +0.15 to −0.04 for Ti and −0.03 for V). The positive charges on C_α and C_γ carbons do not noticeably change. The metal atoms show a large deposit of positive charge, +1.86 for Ti and +1.46 for V, giving them a more electrophilic character than that in $[M(tmtaa)]^+$ fragments.

3.3. The [M(tmtaa)X] and [M(acacen)X], M = Ti, V and X = F, Cl, CH_3 complexes

It is experimentally known that the nature of X influences the redox potential of the metal, which can be a one-electron donor to a variety of substrates, and the reactivity of the systems [35]. Interesting compounds would be those in which the metal in a low oxidation state contains a reactive organometallic functionality, such as metal–halogen or metal–alkyl units. As our last step we are going to investigate the effect of an axial ligand on the $[M(tmtaa)]^+$ and $[M(acacen)]^+$ (M = Ti, V) fragment chemistry, by considering the

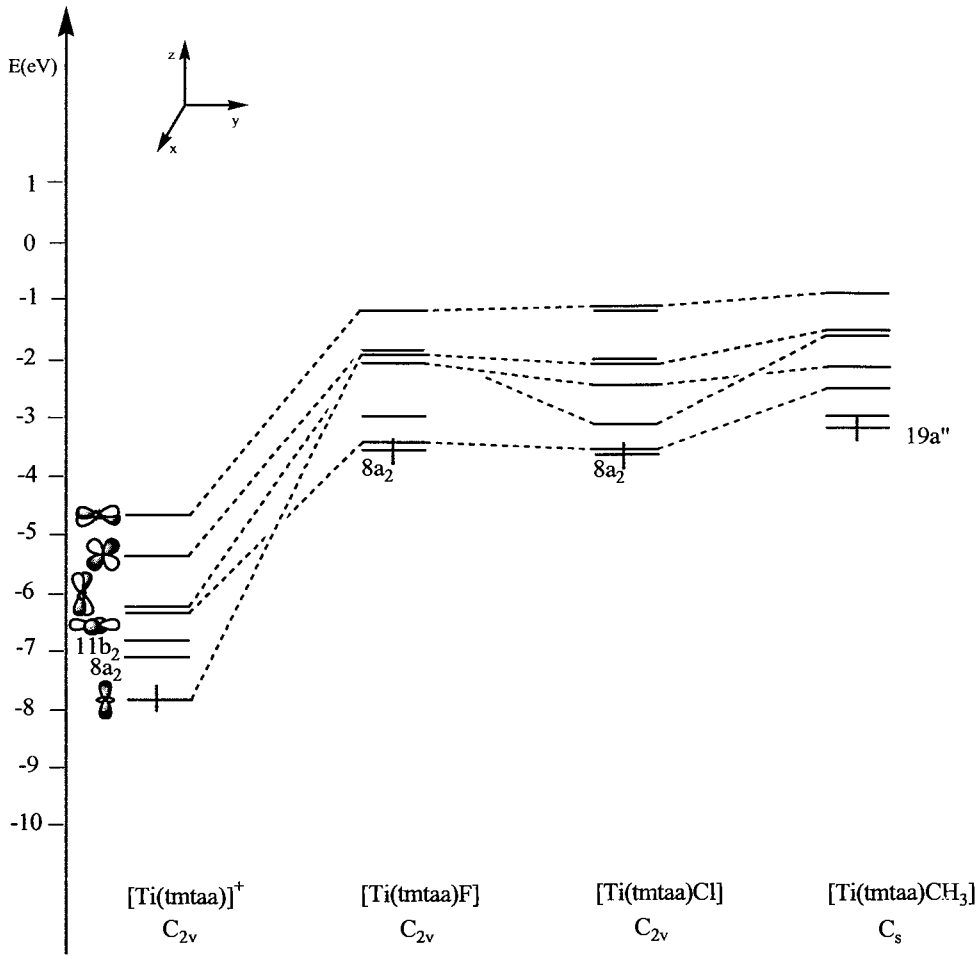

Fig. 3. Molecular orbital diagram for the [Ti(tmtaa)X], X = F, Cl, CH_3, complexes.

ligand series X = F, Cl, CH_3 with σ-donor (CH_3) and π-donor (F, Cl) character. The evidence for stabilization of such M-X functionalities can be explained by analysing the frontier orbitals of the resulting complexes. The geometry of the considered complexes has been partially optimized and the resulting parameters are shown in Table 3, where experimental values, if available, have been also reported for comparison. The calculated parameters can be considered in reasonable agreement with experiment for tmtaa complexes, while for acacen complexes larger deviations from experiment are observed. This can be due to the simplified model systems considered, which constrain the sp^3 carbon to be coplanar with N_2O_2 core. Density functional calculations have been also performed, starting from the corresponding $[M(tmtaa)]^+$, or $[M(acacen)]^+$, and X^- fragments, in order to analyze the type of bonding between these two fragments building up the molecule. In Figs. 3 and 4 molecular orbital diagrams are reported for [Ti(tmtaa)X] and [V(tmtaa)X] (X = F, Cl, CH_3 from the left to the right), respectively, built from the corresponding $[M(tmtaa)]^+$ and X^- fragments. In each complex, of the four lowest lying metal d-orbitals, the d_{z^2} for F and Cl, the $d_{x^2-y^2}$ for CH_3 is pushed up substantially by addition of the fifth ligand X^-. In the F and Cl complexes , the d_{yz} and even more the d_{xz}-orbitals are pushed up significantly, as a consequence of the π-donor effect of these ligands. On comparing the two metals, the titanium shows a stronger π-acceptor character, as the d_{yz}- and d_{xz}-orbitals interact more strongly with the F and Cl π-orbitals and in agreement with the larger electrophilic character (Mulliken charge on Ti in $[Ti(tmtaa)]^+$ + 1.64 vs. + 1.33 on V in $[V(tmtaa)]^+$). As a general trend, the titanium complexes are predicted to have an unpaired electron in one of the two tmtaa π LUMO's character orbital ($^2A_2$ or $^2A''$ ground state), where the other tmtaa LUMO represents the LUMO of the CH_3 complex and $d_{x^2-y^2}$ represents the LUMO of the F and Cl complexes.

The vanadium complexes are predicted to be paramagnetic with two unpaired electrons ($^3A_2$, $^3B_2$, $^3A''$ ground state, respectively) localized in a $d_{x^2-y^2}$ and one of the two tmtaa LUMO's character orbitals for F and Cl, and in d_{z^2}- and d_{yz}-orbitals for CH_3.

From the Mulliken population analysis, it is observed that the nucleophilicity of the metal is enhanced: the

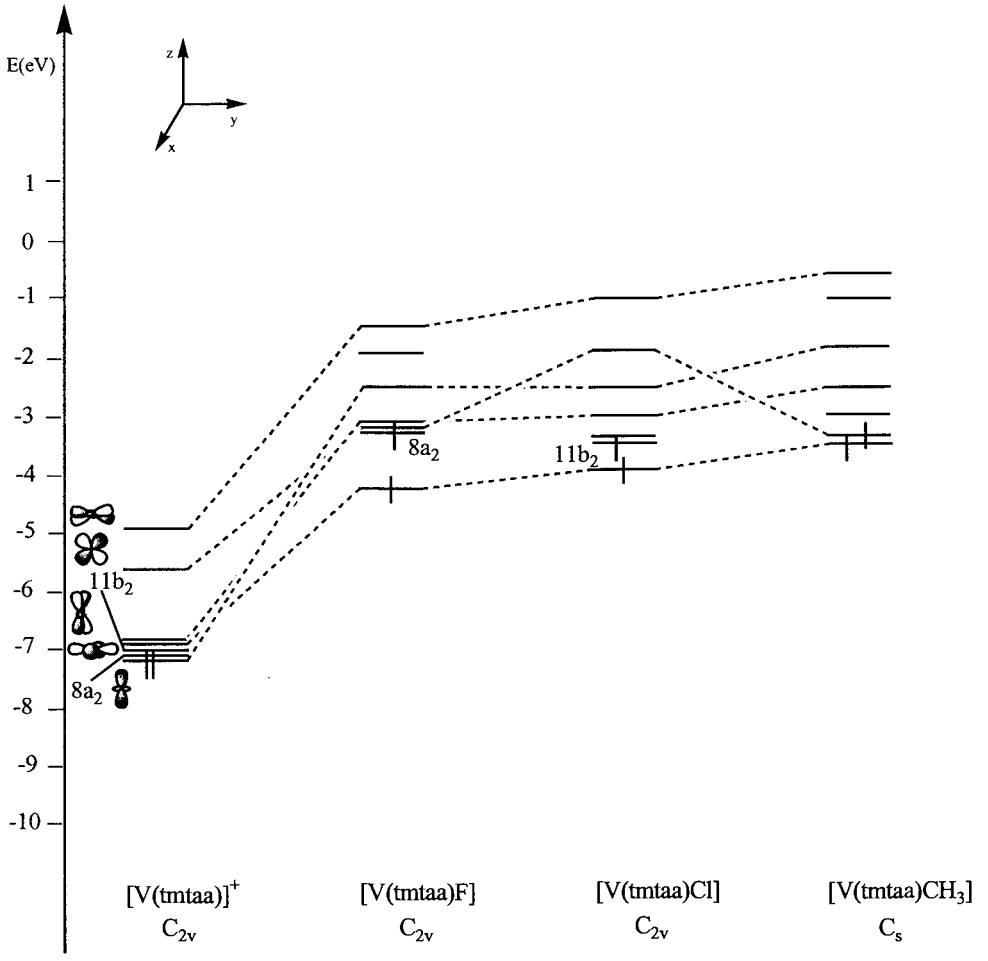

Fig. 4. Molecular orbital diagram for the [V(tmtaa)X], X = F, Cl, CH_3, complexes.

titanium increases its positive charge from +1.64 in $[Ti(tmtaa)]^+$ to +2.01 for F, +1.78 for Cl and +1.84 for CH_3 insertion, the vanadium from +1.33 in $[V(tmtaa)]^+$ to +1.70 for F, +1.43 for Cl and +1.46 for CH_3 insertion.

In Figs. 5 and 6 molecular orbital diagrams are shown for [Ti(acacen)X] and [V(acacen)X] (X = F, Cl, CH_3 from the left to the right), respectively, built from the corresponding $[M(acacen)]^+$ and X^- fragments.

Analogously to the tmtaa fragments, the $d_{x^2-y^2}$ orbital, pointing toward the axial position, is pushed up by the ligand X^- introduction.

In the vanadium complexes, the d_{z^2}- and d_{xy}-orbitals are always singly occupied, with the d_{yz}-orbital being the first LUMO. The frontier orbitals for the titanium complexes show a similar pattern, with the d_{z^2}-orbital being the LUMO and the singly occupied orbital having larger acacen LUMO character.

As a general trend, the introduction of the additional ligand causes a reduction of the metal in the [M(acacen)] based complexes and an oxidation of the metal in the [M(tmtaa)] complexes, in agreement with the frontier orbital patterns shown in Figs. 3–6.

In [Ti(tmtaa)X] complexes the positive charge at the metal ranges from +2.01 (X = F) to +1.78 (X = Cl) and +1.84 ($X = CH_3$) and, due to the unpaired electron now localized on the ligand character $8a_2$ orbital, the positive charge at the imino carbon atoms is reduced from +0.28 to +0.22 (X = F, Cl, CH_3). The *meso*-carbon atoms are not involved in this X coordination process.

In [V(tmtaa)X] compounds the positive charge at the metal varies from +1.70 (X = F) to +1.43 (X = Cl) and +1.46 ($X = CH_3$); the single occupation of the orbitals reflects the tmtaa LUMO character as the positive charge at the iminato carbon atoms reduces significantly from +0.31 to +0.24. Again, no charge variation is seen at the *meso*-carbon atoms. Therefore, the interaction with π- and σ-donor ligands does not underline a different behavior for the $[Ti(tmtaa)]^+$ and $[V(tmtaa)]^+$ fragments.

As for the [Ti(acacen)X] compounds, the 'largest' variation is seen at the metal center, whose positive charge reduces from +1.87 to +1.73 for X = Cl and +1.81 for $X = CH_3$ (for F it remains unchanged), with a slight changing in the charges of the C_β ligand atoms (from −0.13 to −0.17).

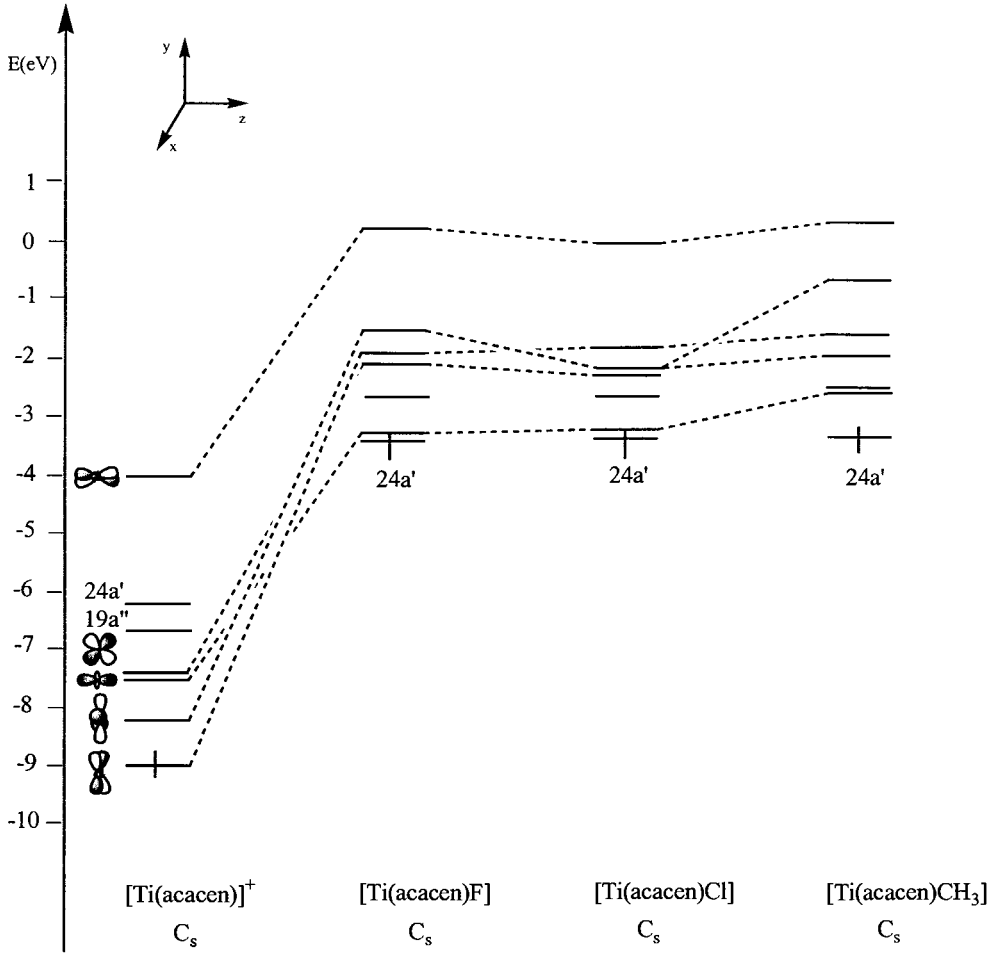

Fig. 5. Molecular orbital diagram for the [Ti(acacen)X], X = F, Cl, CH_3, complexes.

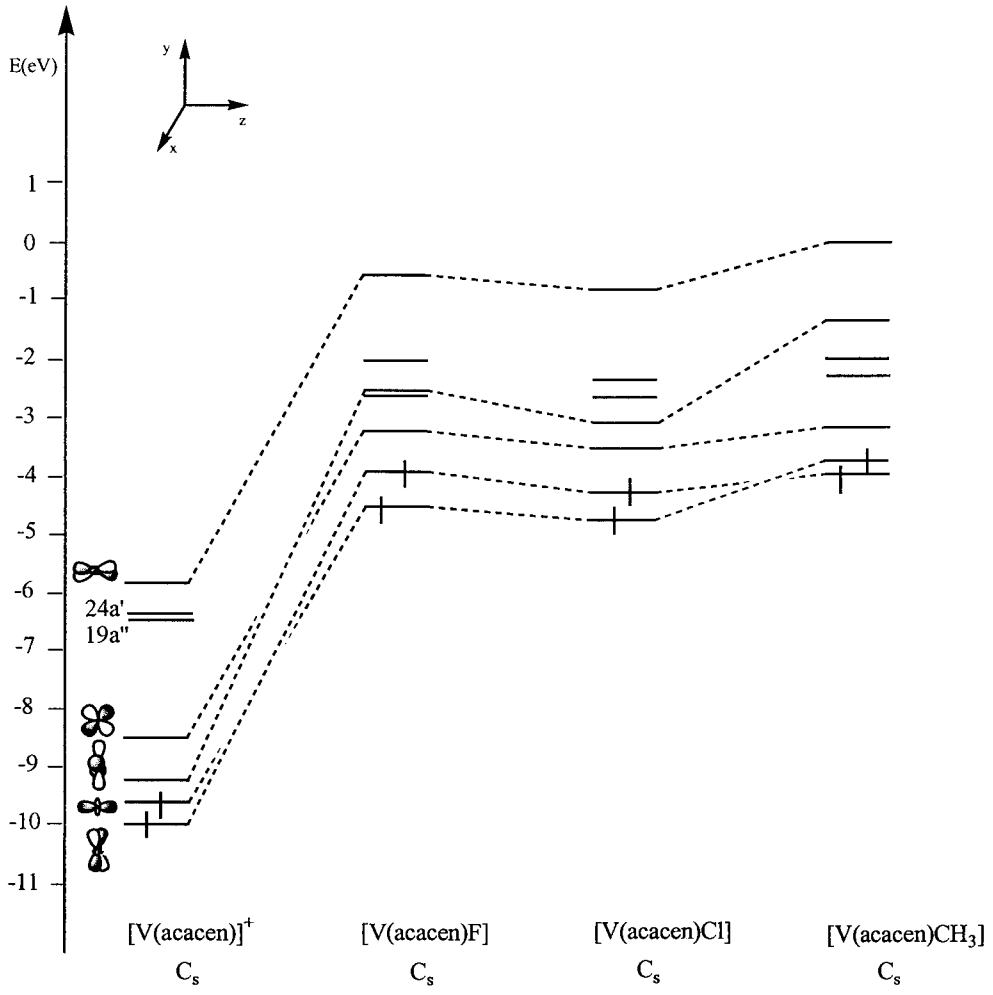

Fig. 6. Molecular orbital diagram for the [V(acacen)X], X = F, Cl, CH_3, complexes.

Finally, the [V(acacen)X] compounds show analogously the largest variation of the metal charge, which ranges from +1.46 to +1.70 for X = F to +1.40 for X = Cl and +1.49 for X = CH_3, and only small at the C_β atom centers (from −0.11 to −0.17).

3.4. The [Mo(acacen)]$_2$ complex

The [Mo(acacen)]$_2$ compound has been experimentally prepared [16] and its molecular structure determined by X-ray crystallography. This compound, together with the [Mo(tmtaa)]$_2$ analogue which has been both synthesized and theoretically studied [17], is of particular interest because it affords the opportunity to compare multiple Mo–Mo bonds in isostructural compounds in which there are no bridging ligands to restrain the metal–metal distances and there are no axial ligands to influence the metal–metal bonding. In addition, the acacen ligands are bulky enough to cause significant repulsive forces between the halves of the molecule, thus causing the staggered conformation of the two monomeric fragments in the dimer, and these ligands have considerable potential for interaction with metal d-orbitals through their delocalized π (bonding) and π* (antibonding) orbitals. The study of the Mo–Mo bonding has been performed by considering the interaction between the two monomeric [Mo(acacen)] species as neutral fragments. To this aim, an unrestricted single point calculation has been carried out on the monomer in the experimental geometry it has in the dimer and in an electronic configuration suitable for the interaction with the other monomer, that is four unpaired electrons which will be involved in the multiple bond when the dimer is formed. The composition of the frontier molecular orbitals is shown in Table 4, where the d-orbitals which can be involved in the multiple bond are explicitly indicated. A coordinate system was defined with the y-axis collinear with the M–M bond, so that the singly occupied lowest lying $d_{x^2-y^2}$ orbital ($18a'$) will give rise to a σ type interaction. Higher in energy, the d_{xy} ($19a'$) orbital will be involved in a π type interaction, the d_{z^2} ($20a'$) orbital in a δ-type one and the highest singly occupied d_{yz} ($17a''$) orbital in a π interaction. The most destabilized d-or-

Table 4
Percentage composition of the lowest unoccupied and highest occupied molecular orbitals of the [Mo(acacen)] monomer complex

	Orbital	E (eV)	% Mo	% N	% O	% $C_{\alpha,\gamma}$	% C_{β}	% C_2H_4
	24a′	0.534				12(p_y)	14(p_y)	
	23a′	0.170	15($5p_y$)+11(6s)					
d_{xz}	19a″	−0.287	51($4d_{xz}$)					
	22a′	−0.819	29($5p_y$)+24(5s)+12(6s)					
	21a′	−2.088	16($4d_{xy}$)	15(p_y)	13(p_y)	40(p_y)		
	18a″ (LUMO)	−2.466	–	18(p_y)	10(p_y)	53(p_y)		
d_{yz} (π)	17a″ (SOMO)	−3.887	63($4d_{yz}$)					
d_{z^2} (δ)	20a′ (SOMO)	−4.345	55($4d_{z^2}$)		11(p_x)			
d_{xy} (π)	19a′ (SOMO)	−4.699	30($4d_{xy}$)+25($4d_{x^2-y^2}$)+14(5s)					
$d_{x^2-y^2}$ (σ)	18a′ (SOMO)	−4.895	44($4d_{x^2-y^2}$)+21($4d_{xy}$)+12($4d_{z^2}$)					
	16a″ (HOMO)	−5.834	13($4d_{yz}$)	16(p_y)	12(p_y)		32(p_y)	
	17a′	−6.013		15(p_y)	12(p_y)		32(p_y)	
	16a′	−6.956			44(p_x)			
	15a″	−7.125			58(p_x)			
	14a″	−8.257		13(p_y)		21(p_y)		
	13a″	−8.464		25(p_x)				

bital is d_{xz} (19a'') which interacts with the π-orbitals of acacen and is therefore not available for the formation of a M–M bond. In Table 5 the frontier molecular orbitals for $[Mo(acacen)]_2$ are shown. We can notice that the 17b_u is predominantly a Mo–Mo σ bonding orbital. The Mo–Mo π bonding is distributed over two orbitals, 18a_g and 17a_u, and the Mo–Mo δ bonding, if it is to occur, should entail the pair of d_{z^2}-orbitals combined with a_g symmetry. The MOs featuring the δ-type interaction are 19a_g and 19b_u orbitals in Table 5. In Fig. 7 the orbital correlation diagram between the two monomeric fragments is shown for $[Mo(acacen)]_2$, where we can note the fully occupied 17b_u, 18a_g, 17a_u and 19a_g (σ, π, π and δ bonding); only two unoccupied antibonding counterparts 19b_u (δ*) and 18b_g (π*) are present in the diagram while the other two lie at much higher energies and are not shown.

Table 5
Percentage composition of the lowest unoccupied and highest occupied molecular orbitals of the $[Mo(acacen)]_2$ complex in terms of monomer fragment [Mo(acacen)]

Orbital	E (eV)	% [Mo(acacen)]
$19b_g$	0.145	45(19a″)
$18b_g$ (π*)	−0.655	40(17a″)
$21b_u$	−0.770	37(19a′)+11(23a′)
$18a_u$	−1.977	49(18a″)
$20b_u$	−2.169	46(21a′)
$17b_g$	−2.586	45(18a″)
$20a_g$	−2.639	29(18a′)+12(20a′)+10(21a′)
$19b_u$ (LUMO) δ*	−3.044	37(20a′)
$19a_g$ (HOMO) δ	−4.070	28(20a′)+13(18a′)
$17a_u$ π	−4.378	44(17a″)
$16b_g$	−5.169	48(16a″)
$18b_u$	−5.173	24(17a′)+21(18a′)
$18a_g$ π	−5.259	33(19a')
$17b_u$ σ	−5.668	26(17a′)+16(18a′)
$17a_g$	−6.165	40(17a′)
$16a_u$	−6.219	41(16a″)
$16a_g$	−6.706	49(16a′)
$16b_u$	−6.851	45(16a′)
$15b_g$	−6.854	49(15a″)

The non-negligible overlap between the $4d_{z^2}$-orbitals indicates unambiguously that a Mo–Mo δ bond exists. The 4d-orbitals, which are more diffuse than the 3d-orbitals, have poorer overlap with the ligand π-orbitals but better overlap with each other. Consequentely, as it has been observed by Cotton et al. [17], the dimolybdenum complex is still a quadruply bonded system, while there is ca. only a triple bond in $[Cr(tmtaa)]_2$. It is also important to note that the calculated HOMO–LUMO energy gap is 1.03 eV, sufficiently high to indicate the existence of a δ-type bond between the Mo, and to suggest that the Mo compound is likely to be fully diamagnetic. Another point of comparison is that Mo–Mo bond length in $[Mo(tmtaa)]_2$ exceeds the Mo–Mo bond length in $[Mo(acacen)]_2$ by only 0.007 Å. The Mo–Mo bond itself is actually a little longer than the values found in many other unbridged Mo_2^{4+} compounds [17] but the small difference can be attributed to the repulsive contacts of the ligands on the two metal atoms that resist any closer approach.

4. Conclusions

The [M(tmtaa)] and [M(acacen)] fragments employed in the organometallic chemistry of early transition metals, namely titanium and vanadium, have been investigated by a density functional approach. The frontier orbitals and the geometrical structure of the two

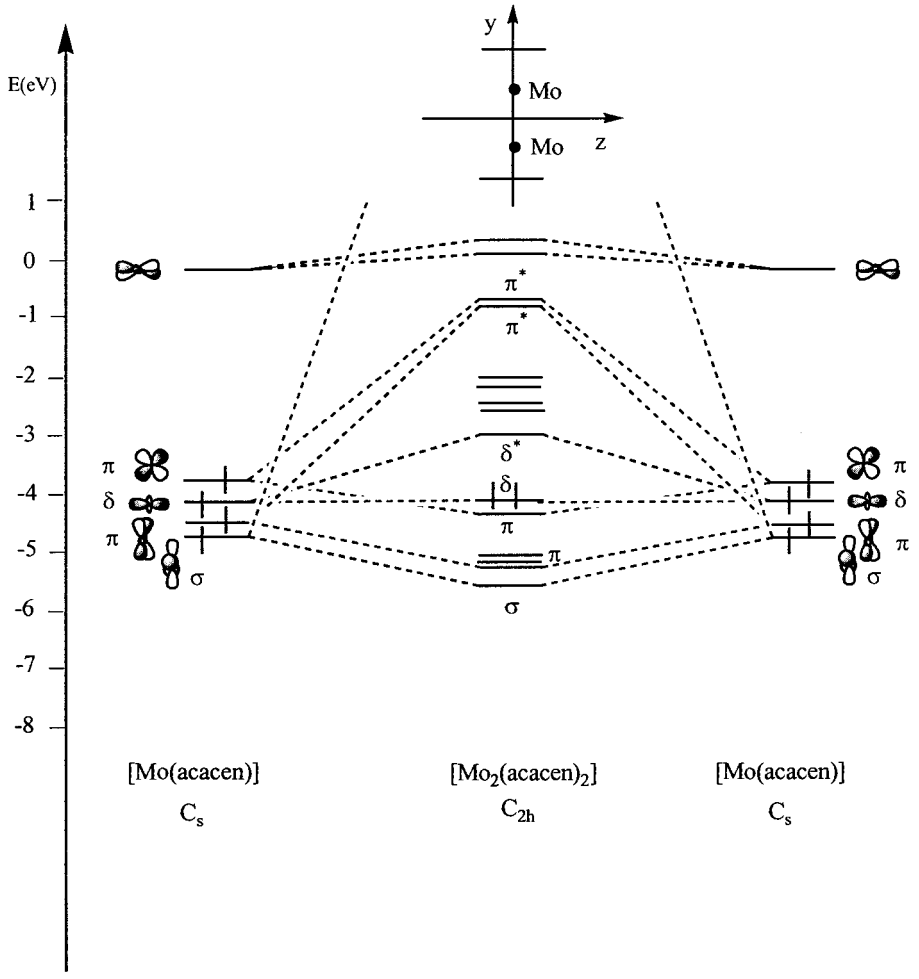

Fig. 7. Molecular orbital diagram for the $[Mo(acacen)]_2$ complexes.

macrocyclic ligands have been compared and the effect of the nature of the metal on the ligand environments has been studied. Some interesting complexes in which the metal in a formal (III) oxidation state contains a reactive organometallic functionality, such as metal–halogen (F and Cl) or metal–alkyl (CH_3) units, have been investigated. Moreover, the $[Mo(acacen)]_2$ dimer has been considered because of its interest as a metal–metal bonded complex with non-bridging ligands restraining the metal–metal distance.

The comparison between Ti and V has shown them to be very similar when bonded to the same ligand. Some analogies between the $[M(tmtaa)]^+$ and $[M(acacen)]^+$ ($M = Ti$, V) fragments have been also found and, consequently, the similar electronic structures of the two fragments are responsible for the similar reactivity pattern when coordinating one additional reactive functionality.

Finally, it has been found that the considered dimolybdenum complex is a stable, diamagnetic quadruply bonded system, which strongly resembles the isostructural analogue $[Mo(tmtaa)]_2$.

Acknowledgements

The authors thank Progetto Finalizzato CNR Materiali Speciali per Tecnologie Avanzate II.

References

[1] See for example P. Mountford, Chem. Soc. Rev. 27 (1998) 105.
[2] J.M. McInnes, D. Swallow, A.J. Blake, P. Mountford, Inorg. Chem. 37 (1998) 5970.
[3] See for example J.P. Corden, W. Errington, P. Moore, M.G.H. Wallbridge, Chem. Commun. (1999) 323 and references therein.
[4] Y.N. Belokon, S. Caveda-Cepas, B. Green, N.S. Ikonnikov, V.N. Khrustalev, V.S. Larichev, M.A. Moscalenko, M. North, C. Orizu, V.I. Tararov, M. Tasinazzo, G.I. Timofeeva, L.V. Yashkina, J. Am. Chem. Soc. 121 (1999) 3968 and references therein.
[5] See for example G. Hoshina, M. Tsuchimoto, S. Ohba, Acta Crystallogr. Sect. C (Cr. Str. Comm.) 56 (2000) e190 and references therein.
[6] R. Uemura, M. Tsuchimoto, S. Ohba, Acta Crystallogr. Sect. C. (Cr. Str. Comm) 56 (2000) e199 and references therein.
[7] S. De Angelis, E. Solari, E. Gallo, C. Floriani, A. Chiesi-Villa, C. Rizzoli, Inorg. Chem 31 (1992) 2520.

[8] L. Giannini, E. Solari, S. De Angelis, T.R. Ward, C. Floriani, A. Chiesi-Villa, C. Rizzoli, J. Am. Chem. Soc. 117 (1995) 5801 and references therein.
[9] E. Solari, S. De Angelis, C. Floriani, A. Chiesi-Villa, C. Rizzoli, Inorg. Chem. 31 (1992) 96 and references therein.
[10] E. Gallo, E. Solari, F. Franceschi, C. Floriani, A. Chiesi-Villa, C. Rizzoli, Inorg. Chem. 34 (1995) 2495.
[11] F. Franceschi, E. Gallo, E. Solari, C. Floriani, A. Chiesi-Villa, C. Rizzoli, N. Re, A. Sgamellotti, Chem. Eur. J. 2 (1996) 1466.
[12] E. Solari, C. Maltese, F. Franceschi, C. Floriani, A. Chiesi-Villa, C. Rizzoli, J. Chem. Soc. Dalton Trans. (1997) 2903.
[13] F. Franceschi, E. Solari, C. Floriani, M. Rosi, A. Chiesi-Villa, C. Rizzoli, Chem. Eur. J. 5 (1999) 708.
[14] A. Martin, R. Urhammer, T.G. Gardner, R.F. Jordan, R.D. Rogers, Organometallics 17 (1998) 382 and references therein.
[15] R. Uhrhammer, D.G. Black, T.G. Gardner, J.D. Olsen, R.F. Jordan, J. Am. Chem. Soc. 115 (1993) 8493.
[16] G. Pennesi, C. Floriani, A. Chiesi-Villa, C. Guastini, J. Chem. Soc. Chem. Commun. (1988) 350.
[17] F.A. Cotton, J. Czuchajowska, X. Feng, Inorg. Chem. 29 (1990) 4329.
[18] G. Ricciardi, A. Bavoso, A. Rosa, F. Lelj, Y. Cizov, J. Chem. Soc. Dalton Trans. (1995) (2385) and references therein.
[19] F.A. Cotton, J. Czuchajowska, Polyhedron 9 (1990) 2553.
[20] http://www.scm.com ADF Program System Release 1999.
[21] E.J. Baerends, D.E. Ellis, P. Ros, Chem. Phys. 2 (1973) 41.
[22] L. Versluis, T. Ziegler, J. Chem. Phys. 88 (1988) 322.
[23] G. te Velde, E.J. Baerends, J. Comput. Phys. 99 (1992) 84.
[24] C. Fonseca Guerra, J.G. Snijders, G. te Velde, E.J. Baerends, Theor. Chem. Acc. 99 (1998) 391.
[25] S.H. Vosko, I. Wilk, M. Nusair, Can. J. Phys. 58 (1980) 1200.
[26] J.P. Perdew, Phys. Rev. Sect. B 33 (1986) 8822.
[27] (a) A. Becke, J. Chem. Phys. 84 (1986) 4524;
(b) A. Becke, J. Chem. Phys. 88 (1988) 1053.
[28] J.M. Kerbaol, J.E. Furet, J.E. Guerchais, Y. Le Mest, J.Y. Saillard, J. Sala-Pala, L. Toupet, Inorg. Chem. 32 (1993) 713 and references therein.
[29] K. Tatsumi, R. Hoffmann, Inorg. Chem. 20 (1981) 3771.
[30] M. Mazzanti, C. Floriani, A. Chiesi-Villa, C. Guastini, Inorg. Chem. 25 (1986) 4158.
[31] J.-M. Rosset, C. Floriani, M. Mazzanti, A. Chiesi-Villa, C. Guastini, Inorg. Chem. 29 (1990) 3991.
[32] C. Floriani, E. Solari, F. Corazza, A. Chiesi-Villa, C. Guastini, Angew. Chem. Int. Ed. Engl. 28 (1989) 64.
[33] S. Ciurli, C. Floriani, A. Chiesi-Villa, C. Guastini, J. Chem. Soc. Chem. Commun. (1986) 1401.
[34] C. Floriani, S. Ciurli, A. Chiesi-Villa, C. Guastini, Angew. Chem. Int. Ed. Engl. 26 (1987) 70.
[35] C. Floriani, M. Mazzanti et al., unpublished work.